Journal of Inorganic Biochemistry 229 (2022) 111718

Contents lists available at ScienceDirect

Journal of Inorganic Biochemistry

journal homepage: www.elsevier.com/locate/jinorgbio

An active site at work – the role of key residues in *C. diphteriae* coproheme decarboxylase

Federico Sebastiani [a], Riccardo Risorti [a], Chiara Niccoli [a], Hanna Michlits [b], Maurizio Becucci [a], Stefan Hofbauer [b,**], Giulietta Smulevich [a,c,*]

[a] *Dipartimento di Chimica "Ugo Schiff" (DICUS), Università di Firenze, Via della Lastruccia 3-13, I-50019 Sesto Fiorentino (FI), Italy*
[b] *University of Natural Resources and Life Sciences, Vienna, Department of Chemistry, Institute of Biochemistry, Muthgasse 18, A-1190 Vienna, Austria*
[c] *INSTM Research Unit of Firenze, via della Lastruccia 3, I-50019 Sesto Fiorentino, Italy*

ARTICLE INFO

Keywords:
Resonance Raman
Fe-His strength
Site-directed variants
Prokaryotic heme biosynthesis
Distal histidine
Hemin reconstitution

ABSTRACT

Coproheme decarboxylases (ChdCs) are utilized by monoderm bacteria to produce heme *b* by a stepwise oxidative decarboxylation of the 2- and 4-propionate groups of iron coproporphyrin III (coproheme) to vinyl groups. This work compares the effect of hemin reconstitution versus the hydrogen peroxide-mediated conversion of coproheme to heme *b* in the actinobacterial ChdC from *Corynebacterium diphtheriae* (*Cd*ChdC) and selected variants. Both ferric and ferrous forms of wild-type (WT) *Cd*ChdC and its H118A, H118F, and A207E variants were characterized by resonance Raman and UV–vis spectroscopies.

The heme *b* ligand assumes the same conformation in the WT active site for both the reconstituted and H_2O_2-mediated product, maintaining the same vinyl and propionate interactions with the protein. Nevertheless, it is important to note that the distal His118, which serves as a distal base, plays an important role in the stabilization of the cavity and for the heme *b* reconstitution. In fact, while the access of heme *b* is prevented by steric hindrance in the H118F variant, the substitution of His with the small apolar Ala residue favors the insertion of the heme *b* in the reversed conformation. The overall data strongly support that during decarboxylation, the intermediate product, a monovinyl-monopropionyl deuteroheme, rotates by 90° within the active site. Moreover, in the ferrous forms the frequency of the ν(Fe-$N_{\delta(His)}$) stretching mode provides information on the strength of the proximal Fe-His bond and allows us to follow its variation during the two oxidative decarboxylation steps.

1. Introduction

Coproheme decarboxylases (ChdCs) catalyze the last step of heme *b* synthesis in monoderm bacteria by a two-step oxidative decarboxylation of the two propionate groups of iron coproporphyrin III (coproheme) [1–5]. It was found that this process involves the formation of a monovinyl monopropionyl deuteroheme (MMD) reaction intermediate and its subsequent 90° rotation before the second decarboxylation, and formation of heme *b* [6–12]. Based on molecular dynamics simulations, UV–vis and resonance Raman (RR) spectroscopies, as well as mass spectrometry of actinobacterial wild-type ChdC from *C. diphtheriae* (*Cd*ChdC) and its H118A, H118F, and A207E variants, we have recently shown that the rotation occurs within the protein pocket and not via a release and rebinding mechanism [11]. In fact, unlike the variant H118A, which, as the wild-type (WT) protein, converts coproheme to heme *b,* the substitution of H118 by the bulkier and more hydrophobic phenylalanine sterically prevented the rotation of the MMD intermediate within the active site, most probably by narrowing the substrate access channel and blocking the movement of the propionate at position 6 to reach the position that was originally occupied by the propionate at position 4. Indeed, upon titration with H_2O_2, this variant accumulates exclusively MMD, where only the propionate at position 2 was

Abbreviations: ChdC, coproheme decarboxylase; *Cd*ChdC, coproheme decarboxylase from *Corynebacterium diphtheriae*; *Lm*ChdC, coproheme decarboxylase from *Listeria monocytogenes*; *Sa*ChdC, coproheme decarboxylase from *Staphylococcus aureus*; DyPs, dye-decolorizing peroxidases; Clds, chlorite dismutases; LS, low-spin; HS, high-spin; QS, quantum mixed-spin; 6c, six coordinated; 5c, five coordinated; RR, resonance Raman; MMD, monovinyl mono-propionate deuteroheme; WT, wild-type.

* Corresponding author at: Dipartimento di Chimica "Ugo Schiff" DICUS, Università di Firenze, Via della Lastruccia 3-13, I-50019 Sesto Fiorentino (FI), Italy.
** Corresponding author.
E-mail addresses: stefan.hofbauer@boku.ac.at (S. Hofbauer), giulietta.smulevich@unifi.it (G. Smulevich).

https://doi.org/10.1016/j.jinorgbio.2022.111718
Received 8 November 2021; Received in revised form 14 December 2021; Accepted 1 January 2022
Available online 6 January 2022

converted to a vinyl group. In addition to the catalytic Y135, the distal H118 is important in actinobacterial ChdCs for deprotonation of hydrogen peroxide and, therefore, Compound I formation [12]. This histidine residue is lacking in firmicute ChdCs and is located on a loop that connects the two ferredoxin-like folds, which is decisive for the respective activities of the entire structural superfamily [13]. The length and the shape of this loop differs significantly from dye-decolorizing peroxidases (DyPs) to chlorite dismutases (Clds) to ChdCs and within ChdCs as well, whereas all other secondary structural elements of the two ferredoxin-like folds are highly similar [13]. In *Cd*ChdC this residue has a relatively low flexibility since it is H-bonded to the propionate 7 (Fig. 1). In addition, the introduction of the hydrogen bonding E207 residue on the proximal heme side in the variant A207E resulted in the formation of mainly MMD, with only a small amount of heme *b* forming upon titration with hydrogen peroxide. Clearly, the altered H-bonding prevented MMD rotation within the active site, likely because an H-bond between E207 and the proximal H158 is established in the unrotated MMD form, as suggested by MD simulations [11]. In *Cd*ChdC, as in the other decarboxylases (e.g. from *S. aureus* [14], *Geobacillus stearothermophilus* [15], and *Listeria monocytogenes* [9]), the mechanism used by the protein to favor the rotation of the reaction intermediate within its pocket is not known. In the present work we study the wild-type and the H118A and A207E variants (Fig. 1) reconstituted with heme *b* in order to understand whether heme *b* maintains the same geometry of insertion as that found after titration, i.e., after the 90° rotation of the MMD intermediate. In addition, we extend the study to the ferrous forms of coproheme-, MMD- and heme *b*- complexes, obtained with H_2O_2 titration or reconstitution, in order to complement the information on the behavior of the protein upon reduction and gain insight into on the status of the proximal Fe-His bond strength during decarboxylation.

2. Materials and methods

2.1. Protein purification and expression

Apoprotein expression and purification was performed as previously described [12]. In order to obtain reconstituted heme *b*-*Cd*ChdC, the procedure was adapted in that *E. coli* pellets containing overexpressed wild-type apo-*Cd*ChdC and variants were lysed by ultrasonication in the presence of 0.5 g/L hemin chloride. The hemin solution (5 g/L) was prepared by dissolving approximately 50 mg of hemin chloride in 2 mL of 1 M NaOH and diluted with water to the final volume of 10 mL. In detail, the cell pellet resulting from 750 mL of *E. coli* culture was resuspended in 50 mL of lysis buffer (50 mM phosphate buffer pH 7.4, with 500 mM NaCl, 5% glycerol, and 0.5% Triton X-100). Subsequently hemin chloride was added and the cells were lysed by three one-minute cycles of pulsed ultrasonication (1 s of sonication with 1 s between pulses, 90% power) on ice. The resulting lysate was centrifuged for 30 min at 38720 *g* and 4°C, and the colored supernatant was filtered (0.45 μm pore sized filter) prior to purification via affinity chromatography.

2.2. Sample preparation

Ferric coproheme-*Cd*ChdC samples were prepared by adding free coproheme solution in 0.5 M NaOH) to apo-*Cd*ChdC diluted in 50 mM phosphate buffer, pH 7.0 in a 2:1 apoprotein:coproheme ratio. Ferric coproheme-*Cd*ChdC samples were titrated by adding small aliquots of a 1 mM H_2O_2 solution in 50 mM phosphate buffer, pH 7.0. An interval of 2–10 min was set before adding each H_2O_2 aliquot to ensure that the reaction was complete. No changes in either the UV–vis absorption or RR spectra were observed 24 h after the sample preparation. Although very small amounts of unconverted coproheme remain up to the end of the titration, it was not possible to proceed with further addition of H_2O_2, since an excess of hydrogen peroxide (e.g. > 2 equivalents for the WT) causes degradation of the protein (for details see Ref. [11]).

Ferric heme *b*-*Cd*ChdC samples were prepared as described above and diluted in 50 mM phosphate buffer, pH 7.0. The corresponding ferrous samples were prepared by addition of a freshly prepared sodium dithionite (20 mg/mL) solution to the ferric forms previously degassed with nitrogen. The concentrations were determined as described previously [11] and were in the range of 25–35 μM for all samples.

2.3. Electronic absorption measurements

Electronic absorption measurements were recorded using a 5 mm NMR tube or a 1 mm cuvette at 25°C by means of a Cary60 spectrophotometer (Agilent, Santa Clara, CA, USA) with a resolution of 1.5 nm and 300 nm/min scan rate. The absorption spectra were measured both before and after RR measurements to ensure that no degradation occurred under the experimental conditions used.

For calculation of the second derivative spectra, the Savitzky-Golay method was applied using 15 data points (LabCalc; Galactic Industries, Salem, NH). No changes in the wavelength or in the bandwidth were observed when the number of points was varied. For the sake of

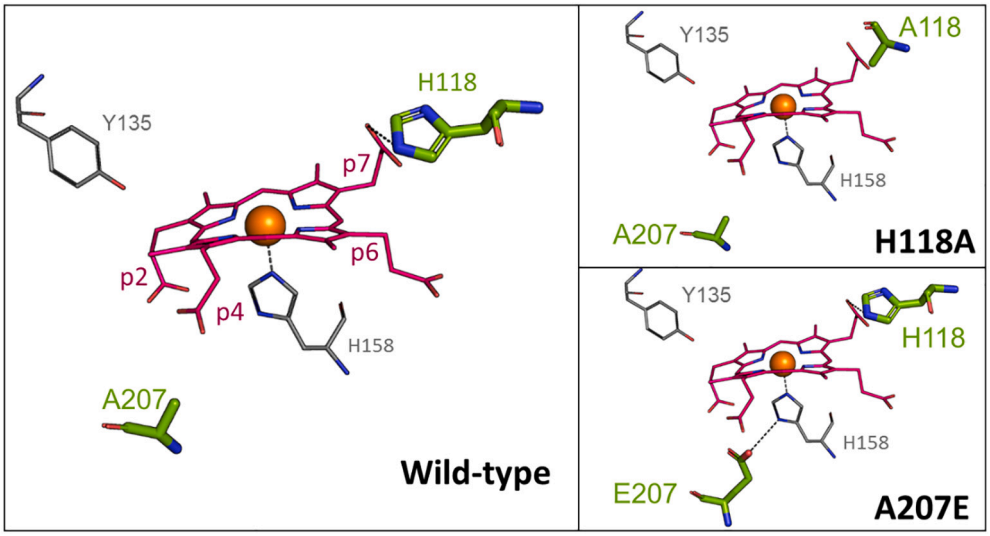

Fig. 1. Active site of the WT coproheme-CdChdC (Protein Data Bank: 6XUC) and the variants H118A and A207E obtained by in silico mutations with PyMOL shown in stick representation. Modified amino acids are shown in green, while distal Y135 and proximal H158 are in grey. (For interpretation of the references to colour in this figure legend, the reader is referred to the web version of this article.)

clarity, the 450–700 nm region in all the absorption spectra is magnified 8-fold.

2.4. Resonance Raman measurements

The resonance Raman (RR) spectra were obtained at room temperature by excitation with the 404.8 nm line of a diode laser (MatchBox Series, Integrated Optics, Vilnius, Lithuania), the 413.1 nm line of a Kr^+ laser (Coherent, Innova 300C; Coherent, Santa Clara, CA, USA) and the 441.6 nm line of a He—Cd laser (Kimmon IK4121R-G, Tokyo, Japan). Backscattered light from a slowly rotating 5 mm NMR tube was collected and focused into a triple spectrometer (consisting of two SpectraPro 2300i instruments working in subtractive mode, and a SpectraPro 2500i instrument in the final stage with gratings of 3600 or 1800 grooves/mm by ActonResearch, Acton, MA, USA), and equipped with a liquid nitrogen-cooled CCD detector. A spectral resolution of 1.2 and 4 cm^{-1} was calculated on the basis of the optical properties of the spectrometer for the 3600 and 1800 grooves/mm gratings, respectively. The RR spectra were calibrated with indene and carbon tetrachloride as standards to an accuracy of 1 cm^{-1} for intense isolated bands. Spectra in polarized light were obtained by inserting a polaroid analyzer between the sample and the entrance slit of the monochromator. The depolarization ratios of the bands at 314 ($\rho = 0.75$) and 460 cm^{-1} ($\rho \approx 0$) of CCl_4 [16] were measured to check the reliability of the measurements.

The power on the samples was 6.5 mW for ferric complexes, and 3.5 / 5.5 mW for ferrous coproheme-complexes / H_2O_2-titrated and heme *b*-complexes, respectively. To avoid sample denaturation, a stream of cooled nitrogen gas was directed toward the rotating sample tube (to stabilized the sample at about 15°C).

All RR measurements were repeated several times under the same conditions to ensure reproducibility. To improve the signal-to-noise ratio, a number of spectra were accumulated and summed only if no spectral differences were noted, as reported in Table S1. The RR spectra were normalized to the intensity of the ν_4 band, at 1352–1357 cm^{-1} for the ferrous samples and at 1370–1374 cm^{-1} for the ferric samples (data not shown), for the high frequency region and to the ν_7 band at 674–678 cm^{-1} in the low frequency region. All spectra were baseline-corrected and were shifted along the ordinate axis in the figures for the sake of clarity.

The curve-fitting analysis of the spectra was performed using a spectral simulation program (LabCalc; Galactic Industries, Salem, NH) with a Lorentzian line shape to determine the peak positions, bandwidths, and intensities with an accuracy of 1 and 0.5 cm^{-1} for the peak positions and the bandwidths, respectively. Since the ν10 and ν(C=C) bands overlap, the fitting procedure with unconstrained parameters was run iteratively: starting from the more well-defined peaks, the widths of the other bands were progressively fixed to the same value for all the samples. As a further check, the widths of the less defined bands were fixed alternatively and were shown to give the same final results. Furthermore, the number of the ν(C=C) bands was obtained by considering both the goodness of the fit in describing the experimental spectra and the measurements performed with polarized light.

3. Results

3.1. Ferric complexes

Recently we have shown that both *Cd*ChdC WT and H118A convert coproheme mainly to heme *b* upon titration with H_2O_2 with small residual amounts of MMD, while the variant A207E accumulates MMD along with a minor amount of heme *b* and H118F generates only MMD [11,12]. We were able to identify the spectroscopic markers of the MMD-*Cd*ChdC complex, showing that it corresponds to a 5-coordinated (5c) high spin (HS) heme. The complex is characterized by a maximum of the Soret band at around 401–402 nm and a band at 586 nm, while the heme *b*-*Cd*ChdC complex of wild-type and the H118A variant is a mixture of 5- and 6-coordinated (6c) HS species (Fig. S1 right) [11]. The RR spectra showed core size markers bands at 1481-2 and 1488-90 cm^{-1} (ν_3, 6c and 5c, respectively), 1568-66 (ν_2, 5c and 6c overlapping), 1609-11 (ν_{10}, 6c) and 1628 (ν_{10}, 5c) cm^{-1}. The A207E variant also gave rise to a mixture of 5c and 6cHS, but the 5cHS was the main species since this variant mainly accumulates MMD, and H118F was a mixture of 5cHS and 5cQS (quantum-mixed spin) species, resulting from coproheme and MMD (Fig. 2 right) [11].

The WT and both H118A and A207E variants reconstituted with heme *b* show UV–vis spectra characteristic of HS species and almost identical to those of the titrated proteins (Fig. S1 left). However, slight changes in the wavelengths of the CT1 band are observed. The band at 586 nm found for the H_2O_2-titrated complexes is not present in any of the UV–vis spectra of the reconstituted proteins, confirming that it derives from the MMD species. It is worth noting that the H118F variant has not been characterized since its heme *b* complex is highly unstable and the ligand is easily released from the protein.

RR is very sensitive at the molecular level and provides information on the heme coordination and spin states via the core size marker bands in the 1300–1700 cm^{-1} wavenumber region [17]. In addition, the characteristic side chains of heme *b* (i.e., *the* vinyl groups on pyrrole rings A and B and the propionate groups on pyrrole rings C and D, which are fundamental for the interactions between the porphyrin and the heme cavity) give rise to bands whose frequencies provide detailed insight into the heme *b* interactions. Information on the two vinyl groups at positions 2 and 4 of the heme are obtained by their ν(C=C) stretching modes between 1615 and 1635 cm^{-1} and the corresponding [$\delta(C_\beta C_a C_b)$] bending modes in the low frequency region. The conjugation between the vinyl substituent and the porphyrin macrocycle induces both a wavenumber decrease of the vinyl ν(C=C) mode and a wavelength increase of the Soret and visible electronic transitions of the heme [18]. Moreover, the frequency of the propionate $\delta(C_\beta C_c C_d)$ bending modes in the low frequency region is strongly influenced by the H-bond interactions between these peripheral groups and the protein [19,20].

The RR spectrum in the high frequency region of the heme *b* reconstituted wild-type appears identical to that obtained by titration with hydrogen peroxide (Fig. 2), demonstrating that it is a mixture of 5c- and 6cHS species. As expected, it is also very similar to those of the reconstituted A207E and H118A variants. A minor amount of 6c low spin (LS) is also present (ν_3 a 1505 cm^{-1}, ν_{10} at 1634 cm^{-1}) only in the reconstituted WT and A207E, while it has not been detected in the H118A variant spectrum. Therefore, we suggest that the H118 residue might bind the Fe atom upon reconstitution.

Upon titration with H_2O_2 the decarboxylation of the propionates and the formation of the vinyl groups was followed by RR spectroscopy, as reported in Ref. [11]. Since the ν(C=C) vinyl stretching modes occur in a crowded region between 1615 and 1635 cm^{-1}, we distinguished the polarized ν(C=C) vinyl stretching modes from the overlapping ν_{10} depolarized bands by measuring the RR spectra in polarized light. The assignment was subsequently confirmed by a curve fitting analysis. After addition of 2 equivalents of hydrogen peroxide to the coproheme complex, the wild-type protein showed two ν(C=C) stretching modes and two $\delta(C_\beta C_a C_b)$ bending modes at 1617/1623 cm^{-1} and 416/421 cm^{-1}, respectively. In the H118A variant broad stretching and bending modes at 1623 and 413 cm^{-1}, respectively, are observed due to overlap of the bands. In the A207E variant, which forms mainly the MMD intermediate, only one stretching and one bending mode at 1624 and 420 cm^{-1}, respectively, were identified (Figs. 2 and 4 and ref [11]).

In the high frequency region, the reconstituted proteins show similar frequencies to their H_2O_2-titrated counterparts, although the vinyl stretching band is broader for the reconstituted A207E and upshifts to 1627 cm^{-1} in the H118A variant (Fig. 2). The spectra taken in polarized light (Fig. S2) show that in the wild-type there are two polarized bands whose frequencies are very close to those observed upon titration [11]. On the contrary, in the H118A spectrum, a third polarized band at 1627 cm^{-1} has been identified which is, therefore, assigned to a third ν(C=C)

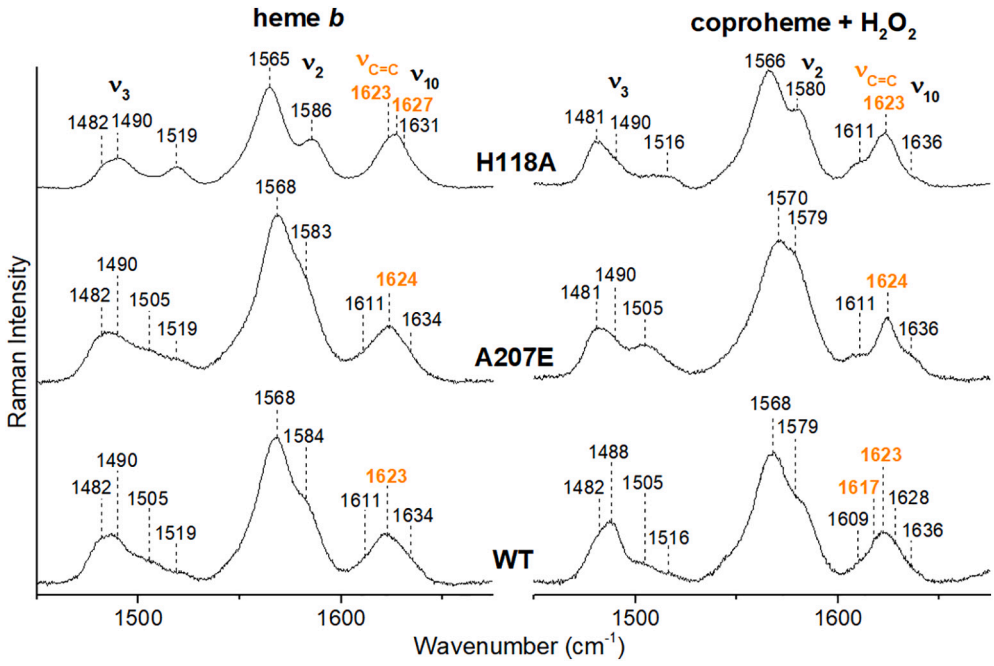

Fig. 2. High frequency RR spectra of the ferric WT *Cd*ChdC-complexes and variants upon reconstitution with heme *b* (left) and upon titration with H_2O_2 (right; from Ref. [11]) (λ_{exc} 413.1 nm). The RR core size marker band wavenumbers are reported in black and vinyl stretching modes ($\nu_{C=C}$) are indicated in orange.

stretching mode. The curve-fitted spectra confirmed that the WT and A207E proteins have two vinyl stretching bands, but three ν(C=C) bands are present in the H118A variant spectrum (Fig. 3 and Table S2). Accordingly, in the low frequency region an intense $\delta(C_\beta C_a C_b)$ vinyl bending vibration was found for the WT and A207E variant, while it is very broad and upshifted in the H118A variant. The $\delta(C_\beta C_a C_b)$ mode can be properly fitted only with three bands at 408, 417, and 424 cm^{-1} for the H118A, and with two bands for the wild-type and A207E at 417 and 423 cm^{-1} (Figs. 4 and S3).

In addition to the bending vibrations of the vinyl groups, in the low frequency region the in-plane and out-of-plane bending modes of the porphyrin together with the bending vibrations of the propionate peripheral groups are found. As for the high frequency region, the reconstituted wild-type and A207E spectra closely resemble the wild-type-titrated spectrum. Therefore, heme *b* insertion does not affect the vinyl orientation, and the porphyrin macrocycle is stabilized by the same H-bond interactions between the propionates in positions 6 and 7 and the heme cavity residues, as upon titration. In fact, an increase (or a decrease) of the number and/or the strength of the H-bonds should have caused a shift to higher (or lower) frequencies of the propionate bending modes [20].

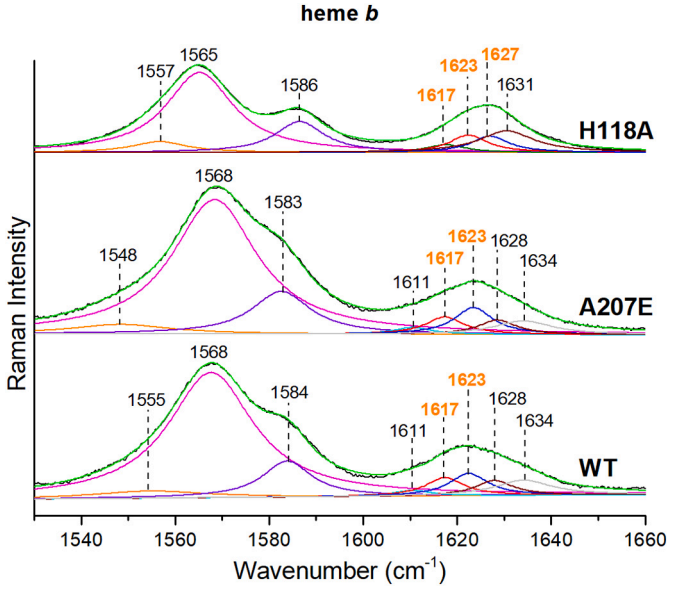

Fig. 3. Curve-fitting analysis of the 1530–1660 cm^{-1} wavenumber region of the ferric reconstituted WT heme *b*-*Cd*ChdC and variants. The RR core size marker band wavenumbers are reported in black and vinyl stretching modes ($\nu_{C=C}$) are indicated in orange. The corresponding bandwidths and assignments are reported in Table S2.

As shown in Fig. 4, the spectrum of the reconstituted H118A variant markedly differs from the other proteins since the ν_8 mode at 342 cm^{-1} is particularly weak, the propionate $\delta(C_\beta C_c C_d)$ bending vibrations shift from 374 to 387 (as in the wild-type and A207E variant) to 368–378 cm^{-1}, and new bands are observed in the 470–520 cm^{-1} region. All these peculiarities, together with the additional ν(C=C) stretching and bending modes, as mentioned above, are reminiscent of the spectrum reported for Mb containing a heme in a reversed conformation [21]. In heme proteins, the coexistence of the two different heme orientations, canonical and reversed, which differ by the rotation of the heme group by 180° about the α,γ-*meso* axis in the protein pocket, has been found in proteins reconstituted with hemin as well as in some native proteins [22]. In the reversed conformation, the order of the two methyl groups at positions 1, 3 and the two vinyl groups at positions 2, 4 of the β carbons of the A and B pyrrole rings is changed compared to the canonical orientation, the methyl groups being located at positions 2 and 4, and the two vinyl groups at positions 1 and 3 (Fig. 5). RR spectroscopy has been found to be particularly informative about the presence of rotational disorder in heme proteins [22]. In fact, among the various intensity and frequency changes observed for selected porphyrin modes [21,23,24], the most peculiar marker is the different disposition of the peripheral vinyl groups in the canonical vs reversed heme insertion which, altering the orientations of the vinyl groups, causes an increase in the frequency of the ν(C=C) vinyl stretching modes [22].

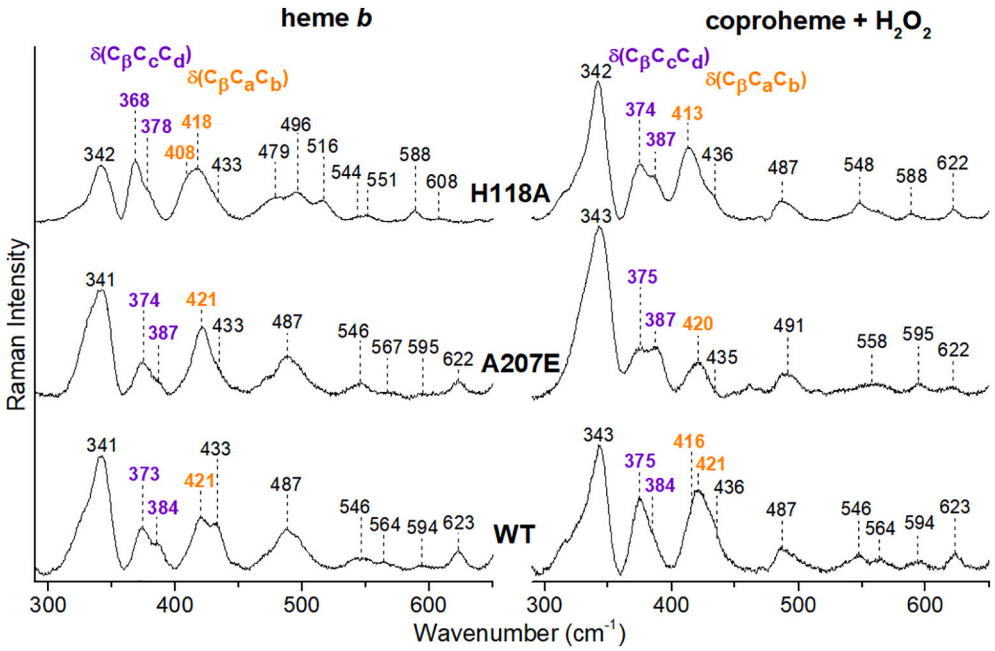

Fig. 4. Low frequency RR spectra of the ferric WT *Cd*ChdC-complexes and variants upon reconstitution with heme *b* (left) and upon titration with H_2O_2 (right; from Ref. [11]) (λ_{exc} 413.1 nm). The propionate bending modes $\delta(C_\beta C_c C_d)$ are indicated in purple and vinyl bending modes $\delta(C_\beta C_a C_b)$ in orange. (For interpretation of the references to colour in this figure legend, the reader is referred to the web version of this article.)

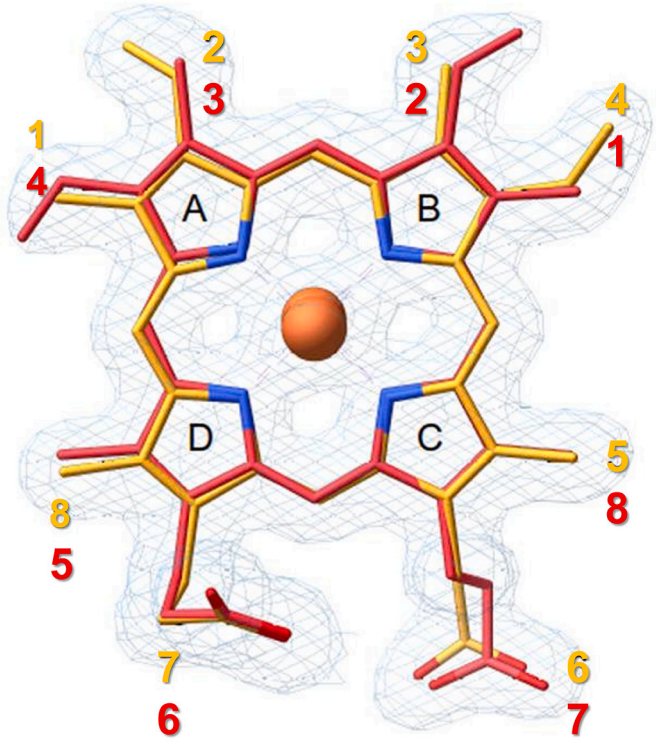

Fig. 5. View of the double heme conformation. In yellow, the canonical heme orientation, in red the reversed heme (adapted from [22]). (For interpretation of the references to colour in this figure legend, the reader is referred to the web version of this article.)

3.2. Ferrous complexes

The UV–vis spectra of the Fe(II) containing coproheme-, MMD-, and heme *b*-complexes, as obtained by H_2O_2 titration or reconstitution, are reported in Fig. S4. All the spectra are characteristic of histidine-ligated 5cHS heme species. Upon reduction, the Soret band red-shifts by about 25 nm with respect to that of the ferric form and an intense broad band in the visible region near 550–560 nm is observed. As for the ferric coproheme complexes [11], due to the lack of the vinyl double bond conjugation with the porphyrin, the electronic absorption spectra of the ferrous coproheme complexes are blue-shifted compared to the heme *b*-containing proteins.

The H_2O_2-titrated Fe(II) complexes (Fig. S4) of the H118F and A207E variants, which have been shown to form only or mainly the MMD intermediate in their ferric form, are characterized by a Soret band maximum in between the fully converted proteins (H118A, wild-type) and the coproheme complexes. Upon reconstitution, only the H118A variant markedly differs, since the Soret band is red-shifted compared to the H_2O_2-titrated forms.

The corresponding RR spectra in the high frequency region of the reduced coproheme, MMD- and heme *b*-complexes (Fig. S5) are characteristic of 5cHS states. Some differences can be noted in the vinyl stretching modes. The H_2O_2-titrated proteins show the vinyl stretching modes at 1619 cm^{-1}, which is more intense in the wild-type and H118A variant than in the A207E variant. This suggests the formation of only one vinyl group in the latter protein. Upon reconstitution, the spectra of the wild-type and A207E variant become similar and almost identical to the wild-type titrated form, confirming that therein complete heme *b* formation has been achieved. As for its ferric forms, an upshift of the vinyl mode is observed in the H118A variant spectrum, being characterized by a very strong and broad band at 1622 cm^{-1}.

The curve-fitted spectra confirm the presence of two vinyl bands in the wild-type and A207E proteins (at 1618 and 1627 cm^{-1} and at 1619 and 1627 cm^{-1}, respectively), while three vinyl stretching modes are found at 1619, 1624 and 1627 cm^{-1} for the H118A variant (Fig. 6), similarly to the ferric form.

Fig. 7 shows the RR spectra of the Fe(II) coproheme-, MMD- and heme *b*-complexes in the low frequency region obtained with 441.6 nm excitation, while the corresponding spectra obtained with a non Soret-resonance excitation (413.1 nm) are reported in Fig. S6. The heme *b*-WT spectra are identical whether obtained by titration with hydrogen peroxide or by reconstitution with hemin. The formation of a heme *b*-complex upon reconstitution of the A207E variant is confirmed by the

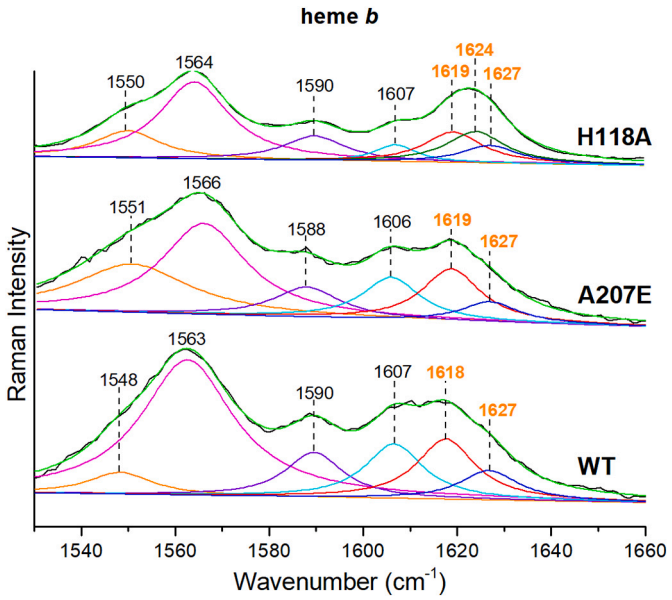

Fig. 6. Curve-fitting analysis of the 1530–1660 cm^{-1} wavenumber region of the ferrous reconstituted WT heme *b*-*Cd*ChdC and variants. The RR core size marker band wavenumbers are reported in black and vinyl stretching modes ($\nu_{C=C}$) are indicated in orange. The corresponding bandwidths and assignments are reported in Table S2.

disappearance of the $\delta(C_\beta C_c C_d)$ propionate vibration at 386 cm^{-1} found in both the coproheme- and the MMD-complexes (Fig. 7). In the titrated H118F variant the presence of MMD is demonstrated by the $\delta(C_\beta C_c C_d)$ propionate vibration at 359 cm^{-1} (observed in the coproheme-complex spectrum, and clearly intensified for 413.1 nm excitation) in addition to the band at 372 cm^{-1}, which is in common with all the other titrated proteins.

The RR low frequency spectrum of a 5cHS ferrous species provides not only information on the propionate and vinyl bending modes, but also on the nature and strength of the proximal iron–imidazole bond via the frequency of the ν(Fe-His) stretching mode, enhanced upon excitation in the Soret band. Its frequency is a sensitive probe of proximal properties of the protein matrix, in particular, to the hydrogen bonding between the N_δ atom of the proximal His and nearby residues [25,26]. In the case of a neutral histidine, i.e., in the absence of an H-bond, the frequency is as low as 200 cm^{-1}, whereas in heme containing peroxidases, where a strong H-bond gives an imidazolate character to the proximal ligand, it is much higher being located in the range 240–260 cm^{-1} [27].

Except for the A207E variant, the other coproheme-complex spectra are characterized by an intense band at 203 cm^{-1}, which loses intensity with 413.1 nm excitation and is, therefore, assigned to the ν(Fe-His) stretching mode (Figs. 7 and S6). Comparison of the spectra for H_2O_2-titration and heme *b* reconstitution indicates that both the formation of the MMD intermediate and its subsequent rotation within the heme cavity (and further decarboxylation) lead to changes in the strength of the Fe-His bond. In fact, in the WT complexes the Fe-His band upshifts to 210 cm^{-1}, but is found at 205 cm^{-1} in the H118F variant upon titration (MMD intermediate) (Fig. 7).

The mutation of the A207 to the negatively charged glutamate, which forms an H-bond to the proximal histidine, clearly has slightly strengthened the Fe-His bond, since its frequency upshifts by 4 cm^{-1} in the coproheme complex as compared to the wild-type. Interestingly, the bond is unaffected by the formation of MMD, and upon reconstitution upshifts only by 1 wavenumber.

The reconstitution of H118A markedly alters the Fe-His bond since its $\nu(\text{Fe-N}_{\delta(\text{His})})$ stretching mode is very high, at 224 cm^{-1}. Moreover, the band frequency and intensity differences noticed in this region for the ferric forms are conserved in the ferrous complexes. In particular, analogous to the reversed deoxy-Mb [23], we clearly observe new bands at 250 (unassigned), 300 (γ_7), 338 (γ_6) cm^{-1} and a downshift of the frequency of the propionate bending mode from 372 to 362 cm^{-1} together with the appearance of a very weak band at 376 cm^{-1}.

4. Discussion

The comparison of the spectral features of the heme *b* – *Cd*ChdC complex, formed upon hydrogen peroxide-mediated conversion of the coproheme complex or via apoprotein-hemin reconstitution, provides important information on the role played by the conserved key-residues of the heme cavity of *Cd*ChdC. The overall data strongly support that during decarboxylation, the intermediate product, a monovinyl-monopropionyl deuteroheme, rotates by 90° within the active site.

The heme *b*-wild-type complexes obtained by hemin reconstitution, either in the ferric or ferrous forms, give rise to almost identical spectra as those obtained by hydrogen peroxide titration. This strongly indicates that two equivalents of H_2O_2 are sufficient to complete decarboxylation of the propionates in positions 2 and 4 to vinyl groups, and the heme *b*-wild-type complex is a mixture of a 5c- and 6cHS hemes in the ferric state and a pure 5cHS in the ferrous form. Moreover, the heme *b* ligand binds the apoprotein maintaining the same vinyl and propionate interactions with the protein surroundings of the cavity as observed for the H_2O_2-mediated reaction.

In the ferrous forms, the $\nu(\text{Fe-N}_{\delta(\text{His})})$ stretching mode frequency provides further information on the strength of the proximal Fe-His interaction. Variations induced by the formation of the MMD reaction

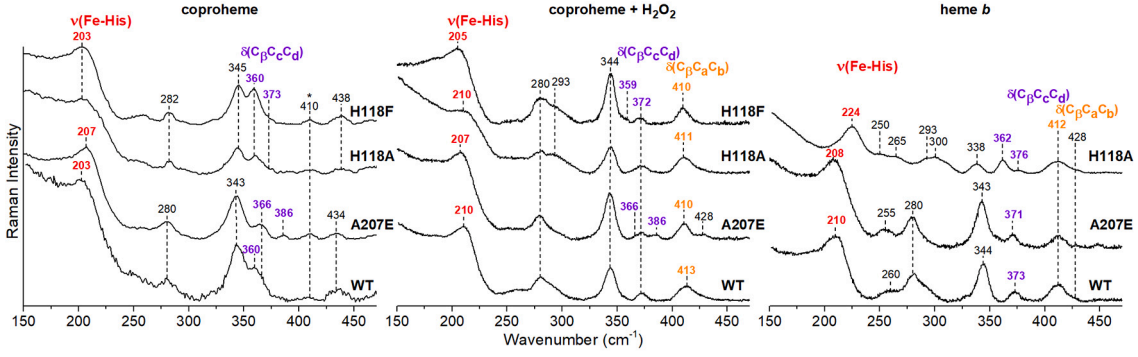

Fig. 7. Low frequency RR spectra of the ferrous forms of the coproheme- (left), H_2O_2 titrated- (middle), and heme *b*-reconstituted (right) complexes of WT *Cd*ChdC and variants (λ_{exc} 441.6 nm). The propionate bending modes $\delta(C_\beta C_c C_d)$ are indicated in purple, the vinyl bending modes $\delta(C_\beta C_a C_b)$ in orange and the ν(Fe-His) stretching mode in red. As the coproheme complexes are unstable in the laser beam, the weak vinyl bending band formed upon increasing laser irradiation time is indicated by an asterisk. (For interpretation of the references to colour in this figure legend, the reader is referred to the web version of this article.)

intermediate and heme *b* during the decarboxylation reaction of the propionates can be detected.

Table 1 compares the ν(Fe-$N_{\delta(His)}$) frequencies of the ferrous coproheme and heme *b*-complexes of the WT and its variants. For the wild-type the ν(Fe-$N_{\delta(His)}$) stretching mode in the coproheme complex is at 203 cm^{-1}. The decarboxylation of the first propionate (p2) with the formation of unrotated MMD, slightly strengthens the Fe-His bond, as suggested by the 2 wavenumbers upshift observed in the H118F variant upon addition of H_2O_2. After the hydrogen peroxide mediated formation of heme *b* or after heme *b* reconstitution, the Fe-His bond is strengthened and the ν(Fe-$N_{\delta(His)}$) is shifted to 210 cm^{-1} in the WT. Interestingly, the frequency of this mode in other decarboxylases belonging to the Firmicutes clade is higher (214 cm^{-1}) and no change in frequency (*L. monocytogenes*) [28] or only a slight upshift (2 cm^{-1} in *S. aureus*) [29] was found upon H_2O_2 titration of the coproheme complexes. Subtle changes are observed for the variants. While the coproheme complexes of the H118 variants are characterized by a ν(Fe-$N_{\delta(His)}$) stretching mode frequency at 203 cm^{-1} as in the WT, in the A207E variant the novel H-bond between the glutamate 207 residue and the N_ε atom of the proximal histidine 158, slightly strengthens the Fe-His bond, upshifting the ν(Fe-$N_{\delta(His)}$) mode to 207 cm^{-1}, both in coproheme and in the unrotated MMD intermediate complexes, and 208 cm^{-1} upon heme *b* reconstitution. The new H-bond helps to mimic the Clds which are characterized by a proximal H-bonding network involving the iron coordinating histidine via a conserved glutamate to the propionate groups of heme *b*, which strongly regulates the active site for efficient catalysis of chlorite degradation [30,31]. The ν(Fe-$N_{\delta(His)}$) frequencies of the heme *b*-Clds are, however, much higher, ranging from 222 cm^{-1} [32], 226 cm^{-1} [30], to 229 cm^{-1} [33]. Therefore, although the mutation affects the oxidative formation of heme *b* in the A207E variant [11], it does not result in a significant change in its ν(Fe-His) frequency with respect to the heme *b*-*Cd*ChdC wild-type.

The present results clearly provide evidence that the H118 residue is not only important in actinobacterial ChdCs for deprotonation of hydrogen peroxide and therefore Compound I formation [12], but it is also involved in heme binding. In fact, the steric encumbered Phe residue in the H118F variant dramatically weakens the binding affinity for heme *b,* preventing reconstitution. Moreover, an intriguing and unexpected result was the discovery that in the H118A variant the replacement of the H118 residue with the small apolar Ala residue causes heme rotational disorder and heme *b* enters mainly in the reversed conformation. In general, the amount of reversed heme detected in natural heme proteins is quite small and its presence depends not only on the specific globin, but also on the oxidation and ligation states of the heme iron, and on the heme pocket environment [22,34]. In the present case, both ferric and ferrous forms behave similarly. The presence of heme *b* in a reversed conformation might be ascribed to a hydrophobic interaction between apolar residues and the porphyrin ring, which has been found to be particularly relevant in determining such forms [35]. The insertion of heme *b* in a reversed conformation in the H118A variant alters the RR signatures of many vibrations of the porphyrin and vinyl groups, as previously described for Mb [21,23,24]. However, unlike the case of reversed Mb, in the H118A variant it strengthens the Fe-His bond, as clearly observed by its shift to 224 cm^{-1}, and the marked upshift of the Soret band maximum. The distal H118 in *Cd*ChdC is located on a flexible loop, whose orientation is specific only for actinobacterial ChdCs, it remains unclear if there are residues on this loop in the well-studied firmicute ChdCs (e.g. *Lm*ChdC from L. *monocytogenes* or *Sa*ChdC *from S. aureus*) which have a similar role [8,36]. In firmicute ChCds, the active site architecture is determined by a distal glutamine residue (Q187 in *Lm*ChdC,) and a nearby methionine residue (M149 in *Lm*ChdC). Both residues are only conserved in firmicute ChdCs and dictate whether an open or closed active site conformation is formed. Therefore, they are involved in the hydrogen peroxide stabilization during turnover [8,36]. The flexible loop in firmicute ChdCs, linking the N- and C-terminal domains is significantly longer and carries also one histidine (H117 in *Lm*ChdC) [13,37], which is, according to the solved crystal structure, far away (17 Å) from the coproheme iron [9] and is thus unlikely to perform the same roles as H118 in *Cd*ChdC.

Table 1
ν(Fe-$N_{\delta(His)}$) frequencies (cm^{-1}) of the ferrous coproheme-, H_2O_2 titrated- and reconstituted heme *b*-complexes of WT-*Cd*ChdC and variants.

	ν[Fe-$N_{\delta(His)}$] stretching mode (cm^{-1})		
	coproheme	+ H_2O_2	+ heme *b*
		MMD heme *b*	heme *b*
Wild-type	203	210	210
A207E	207	207	208
H118A*	203	210	224*
H118F	203	205	

* reversed.

Funding sources

This project was supported by Fondazione Cassa Risparmio di Firenze, Grant 2020.1397 (G.S.) and the Austrian Science Fund, FWF standalone project: P29099 (SH), and the FWF doctoral program "Biomolecular Technology of Proteins" (BioToP) W1224 (HM).

Declaration of Competing Interest

The authors declare that they have no known competing financial interests or personal relationships that could have appeared to influence the work reported in this paper.

Acknowledgment

We thank Dr. B.D. Howes for helpful discussions.

Appendix A. Supplementary data

Supplementary data to this article can be found online at https://doi.org/10.1016/j.jinorgbio.2022.111718.

References

[1] S.A. Lobo, A. Scott, M.A. Videira, D. Winpenny, M. Gardner, M.J. Palmer, S. Schroeder, A.D. Lawrence, T. Parkinson, M.J. Warren, L.M. Saraiva, Mol. Microbiol. 97 (2015) 472–487.
[2] H.A. Dailey, S. Gerdes, T.A. Dailey, J.S. Burch, J.D. Phillips, Proc. Natl. Acad. Sci. U. S. A. 112 (2015) 2210–2215.
[3] X. Huang, J.T. Groves, Chem. Rev. 118 (2018) 2491–2553.
[4] F.P. Guengerich, F.K. Yoshimoto, Chem. Rev. 118 (2018) 6573–6655.
[5] B. Li, J. Bridwell-Rabb, Biochemistry 58 (2019) 85–93.
[6] G. Layer, Biochim. Biophys. Acta Mol. Cell Res. 1868 (2021) 118861.
[7] H.A. Dailey, T.A. Dailey, S. Gerdes, D. Jahn, M. Jahn, M.R. O'Brian, M.J. Warren, Microbiol. Mol. Biol. Rev. 81 (2017) e00048-16.
[8] A.I. Celis, G.H. Gauss, B.R. Streit, K. Shisler, G.C. Moraski, K.R. Rodgers, G.S. Lukat-Rodgers, J.W. Peters, J.L. DuBois, J. Am. Chem. Soc. 139 (2017) 1900–1911.
[9] L. Milazzo, T. Gabler, D. Pühringer, Z. Jandova, D. Maresch, H. Michlits, V. Pfanzagl, K. Djinović-Carugo, C. Oostenbrink, P.G. Furtmüller, C. Obinger, G. Smulevich, S. Hofbauer, ACS Catal. 9 (2019) 6766–6782.
[10] Y. Zhang, J. Wang, C. Yuan, W. Liu, H. Tan, X. Li, G. Chen, Phys. Chem. Chem. Phys. 22 (2020) 1617–1624.
[11] F. Sebastiani, H. Michlits, B. Lier, M. Becucci, P.G. Furtmüller, C. Oostenbrink, C. Obinger, S. Hofbauer, G. Smulevich, Biophys. J. 120 (2021) 3600–3614.
[12] H. Michlits, B. Lier, V. Pfanzagl, K. Djinović-Carugo, P.G. Furtmüller, C. Oostenbrink, C. Obinger, S. Hofbauer, ACS Catal. 10 (2020) 5405–5413.
[13] S. Hofbauer, V. Pfanzagl, H. Michlits, D. Schmidt, C. Obinger, P.G. Furtmüller, Biochim. Biophys. Acta Proteins Proteomics 1869 (2021) 140536.
[14] B.R. Streit, A.I. Celis, G.C. Moraski, K.A. Shisler, E.M. Shepard, K.R. Rodgers, G. S. Lukat-Rodgers, J.L. DuBois, J. Biol. Chem. 293 (2018) 3989–3999.
[15] G. Tian, G. Hao, X. Chen, Y. Liu, Inorg. Chem. 60 (17) (2021) 13539–13549.
[16] W.F. Murphy, M.V. Evans, P. Bender, J. Chem. Phys. 47 (1967) 1836–1839.
[17] T.G. Spiro, X.-Y. Li, Resonance Raman spectroscopy of metalloporphyrins, in: T. G. Spiro (Ed.), Biological Applications of Raman Spectroscopy 3, John Wiley and Sons Inc., New York, 1988, pp. 1–37.
[18] M.P. Marzocchi, G. Smulevich, J. Raman Spectrosc. 34 (2003) 725–736.

[19] D.S. Gottfried, E.S. Peterson, A.G. Sheikh, J.Q. Wang, M. Yang, J.M. Friedman, J. Phys. Chem. US 100 (1996) 12034–12042.
[20] E.S. Peterson, J.M. Friedman, E.Y. Chien, S.G. Sligar, Biochemistry 37 (1998) 12301–12319.
[21] F. Rwere, P.J. Mak, J.R. Kincaid, Biopolymers 89 (2008) 179–186.
[22] F. Sebastiani, L. Milazzo, C. Exertier, M. Becucci, G. Smulevich, J. Raman Spectrosc. 52 (2021) 2536–2549.
[23] F. Rwere, P.J. Mak, J.R. Kincaid, Biochemistry 47 (2008) 12869–12877.
[24] F. Rwere, P.J. Mak, J.R. Kincaid, J. Raman Spectrosc. 45 (2014) 97–104.
[25] P. Stein, M. Mitchell, T.G. Spiro, J. Am. Chem. Soc. 102 (1980) 7795–7797.
[26] T. Kitagawa, in: T.G. Spiro (Ed.), Biological Applications of Raman Spectroscopy: Resonance Raman Spectra of Hemes and Metalloproteins vol. 3, Wiley, New York, 1988, pp. 97–131.
[27] G. Smulevich, B.D. Howes, E. Droghetti, in: E. Raven, B. Dunford (Eds.), Heme Peroxidases, RSC Metallobiology Series, The Royal Society of Chemistry, 2016, pp. 61–98.
[28] S. Hofbauer, G. Mlynek, L. Milazzo, D. Pühringer, D. Maresch, I. Schaffner, P. G. Furtmüller, G. Smulevich, K. Djinović-Carugo, C. Obinger, FEBS J. 283 (2016) 4386–4401.
[29] B.R. Streit, A.I. Celis, K. Shisler, K.R. Rodgers, G.S. Lukat-Rodgers, J.L. DuBois, Biochemistry 56 (2017) 189–201.
[30] S. Hofbauer, B.D. Howes, N. Flego, K.F. Pirker, I. Schaffner, G. Mlynek, K. Djinović-Carugo, P.G. Furtmüller, G. Smulevich, C. Obinger, Biosci. Rep. 36 (2016) e00312.
[31] S. Hofbauer, K. Gysel, M. Bellei, A. Hagmüller, I. Schaffner, G. Mlynek, J. Kostan, K.F. Pirker, H. Daims, P.G. Furtmüller, G. Battistuzzi, K. Djinović-Carugo, C. Obinger, Biochemistry 53 (2014) 77–89.
[32] B.R. Streit, B. Blanc, G.S. Lukat-Rodgers, K.R. Rodgers, J.L. DuBois, J. Am. Chem. Soc. 132 (2010) 5711–5724.
[33] A.I. Celis, Z. Geeraerts, D. Ngmenterebo, M.M. Machovina, R.C. Kurker, K. Rajakumar, A. Ivancich, K.R. Rodgers, G.S. Lukat-Rodgers, J.L. DuBois, Biochemistry 54 (2015) 434–446.
[34] L. Milazzo, C. Exertier, M. Becucci, I. Freda, L.C. Montemiglio, C. Savino, B. Vallone, G. Smulevich, FEBS J. 287 (2020) 4082–4097.
[35] S. Juillard, S. Chevance, A. Bondon, G. Simonneaux, Biochim. Biophys. Acta 1814 (2011) 1188–1194.
[36] L. Milazzo, S. Hofbauer, B.D. Howes, T. Gabler, P.G. Furtmüller, C. Obinger, G. Smulevich, Biochemistry 57 (2018) 2044–2057.
[37] V. Pfanzagl, L. Holcik, D. Maresch, G. Gorgone, H. Michlits, P.G. Furtmüller, S. Hofbauer, Arch. Biochem. Biophys. 640 (2018) 27–36.